Journal of Hazardous Materials 169 (2009) 221–227

Contents lists available at ScienceDirect

Journal of Hazardous Materials

journal homepage: www.elsevier.com/locate/jhazmat

Template-free fabrication of hierarchically flower-like tungsten trioxide assemblies with enhanced visible-light-driven photocatalytic activity

Jiaguo Yu*, Lifang Qi

State Key Laboratory of Advanced Technology for Material Synthesis and Processing, Wuhan University of Technology, Luoshi Road 122#, Wuhan, Hubei 430070, PR China

ARTICLE INFO

Article history:
Received 13 December 2008
Received in revised form 14 March 2009
Accepted 18 March 2009
Available online 27 March 2009

Keywords:
Tungsten trioxide
Hierarchical assemblies
Flower-like
Photocatalytic activity
Visible-light
Rhodamine B

ABSTRACT

Hierarchically flower-like tungsten trioxide assemblies were fabricated on a large scale by a simple hydrothermal treatment of sodium tungstate in aqueous solution of nitric acid. The as-prepared samples were characterized by X-ray diffraction, scanning electron microscopy and N_2 adsorption–desorption measurements. The photocatalytic activity was evaluated by photocatalytic decolorization of rhodamine B aqueous solution under visible-light irradiation. It was found that the three-dimensional tungsten trioxide assemblies were constructed from two-dimensional layers, which were further composed of a large number of interconnected lathy nanoplates with different sizes. Such flower-like assemblies exhibited hierarchically porous structure and higher visible-light photocatalytic activity than the samples without such hierarchical structures due to their specific hierarchical pores that served as the transport paths for light and reactants. After five recycles for the photodegradation of RhB, the catalyst did not exhibit any great loss in activity, confirming hierarchically flower-like tungsten trioxide was stability and not photocorroded. This study may provide new insight into environmentally benign preparation and design of novel photocatalytic materials and enhancement of photocatalytic activity.

1. Introduction

In recent years, a great deal of effort has been devoted to solving the seriously environmental pollution problems [1–4]. Compared with conventional oxidation processes, oxide semiconductor photocatalysis has several obvious advantages, such as complete mineralization of the pollutants, application of the near-UV or solar light, no addition of other chemicals, operation at near room temperature and low cost [5–9]. Among various oxide semiconductor photocatalysts, TiO_2 is most widely used because of its biological and chemical inertness, strong oxidizing power, nontoxicity and long-term stability against photo and chemical corrosion [10–16]. However, TiO_2 can be only activated under ultraviolet irradiation ($\lambda < 380$ nm) due to its large band gap (3.2 eV). Usually, sunlight contains about 4% ultraviolet light [15,16]. So, it is of great interest to develop new visible-light photocatalysts to extend their photocatalytic applications from ultraviolet to visible-light range.

Tungsten trioxide (WO_3) and hydrated tungsten oxide ($WO_3 \cdot nH_2O$, $n = 1/3$, etc.) have been widely studied because of their interesting electrochemistry properties and applications as solar energy devices, photochromic devices, chemical sensors and catalytic properties [17–23]. As one of the semiconductor photocatalysts, tungsten trioxide has several advantages, such as (1) innocuity, (2) chemically inert and photoelectrochemical stability in aqueous media over a very wide pH range, (3) lower optical band gap (~2.7 eV), resulting in a wider response of the solar spectrum [24–27]. Guo et al. [28] have reported the high photocatalytic capability of self-assembled nanoporous WO_3. Morates et al. [24] studied photocatalytic activity of nanocrystalline WO_3 prepared by a combustion reaction method. Very recently, we have reported fabrication of WO_3 hollow microspheres and their photocatalytic activity for the decolorization of methyl orange aqueous solution [22]. However, there are few reports on the preparation and photocatalytic activities of hierarchically flower-like tungsten trioxide assemblies. In this work, we describe a simple and environmentally benign method for the fabrication of hierarchically flower-like tungsten trioxide assemblies and their formation mechanism and photocatalytic activity.

2. Experimental

2.1. Sample preparation

All the chemicals used in this study were used as received from Shanghai Chemical Regent Factory of China without further purification. Distilled water was used in all experiments. Hierarchically flower-like tungsten trioxide assemblies were prepared through a simple hydrothermal method. In a typical experiment, 1.98 g of

* Corresponding author. Tel.: +86 27 87871029; fax: +86 27 87879468.
E-mail address: jiaguoyu@yahoo.com (J. Yu).

0304-3894/$ – see front matter © 2009 Elsevier B.V. All rights reserved.
doi:10.1016/j.jhazmat.2009.03.082

Table 1
Experimental conditions of preparation of the samples.

Sample no.	[Na_2WO_4] (mol/L)	Acid (mol/L)	R	Temp. (°C)	Time (h)
W1	0.006	HNO_3 (0.009)	1.5	160	24
W2	0.006	HNO_3 (0.012)	2	160	24
W3	0.006	HNO_3 (0.018)	3	160	24
W4	0.003	HNO_3 (0.006)	2	160	24
W5	0.009	HNO_3 (0.018)	2	160	24
W6	0.006	HCl (0.012)	2	160	24
W7	0.006	H_2SO_4 (0.012)	2	160	24
W8	0.006	HNO_3 (0.000)	0	160	24
W9	0.006	HNO_3 (0.006)	1	160	24

sodium tungstate ($Na_2WO_4{\cdot}2H_2O$) was first dissolved in 58.5 mL of distilled water, then 1.5 mL of HNO_3 aqueous solution (8 mol/L) was added dropwise into the above solution under magnetic stirring. The light yellow aqueous solution obtained after continuous 10 min of vigorous stirring was transferred to a 100-mL Teflon-lined autoclave, which was then filled with water up to 60% of the total volume. The autoclave was sealed and kept at 160 °C for 24 h. After reaction, the pH value of the solution was below 1.0. The white precipitate was collected and washed with distilled water and anhydrous alcohol for three times. The final product was dried in a vacuum at 80 °C for 12 h. Control experiments, as above, but with changes in kind of acid, reaction times from 0 to 24 h, concentration of Na_2WO_4 from 0.003 to 0.009 M and molar ratio of HNO_3 to Na_2WO_4 (R) from 0 to 3 were also undertaken, as presented in Table 1.

2.2. Characterization

X-ray diffraction (XRD) patterns obtained on an X-ray diffractometer (type HZG41B-PC) using Cu Kα irradiation at a scan rate of 0.05° 2θ s^{-1} were used to determine the phase structures of the obtained samples. The accelerating voltage and the applied current were 40 kV and 80 mA, respectively. The morphology observation was performed on a S4800 field emission scanning electron microscopy (FESEM, Hitachi, Japan) at an accelerating voltage of 5 kV and linked with an Oxford Instruments X-ray analysis system. The Brunauer–Emmett–Teller (BET) surface area (S_{BET}) of the powders was analyzed by nitrogen adsorption in a Micromeritics ASAP 2020 nitrogen adsorption apparatus (USA). All samples were degassed at 100 °C prior to nitrogen adsorption measurements. The BET surface area was determined by a multipoint BET method using the adsorption data in the relative pressure (P/P_0) range of 0.05–0.25. Desorption isotherm was used to determine the pore size distribution via the Barret–Joyner–Halender (BJH) method, assuming a cylindrical pore modal [29,30]. The nitrogen adsorption volume at the relative pressure (P/P_0) of 0.972 was used to determine the pore volume and average pore size.

2.3. Measurement of photocatalytic activity

Rhodamine B (RhB), one of the N-containing dyes, which are resistant biodegradation and direct photolysis, is a popular probe molecule in the heterogeneous photocatalysis reaction. The evaluation of photocatalytic activity of the prepared samples for the photocatalytic decolorization of RhB aqueous solution was performed at ambient temperature, as reported in our previous studies [31]. Experimental procedures were as follows: the catalysts were prepared by coating an aqueous suspension of WO_3 powders onto one dishes with diameters of about 7.0 cm. The weight of catalysts used in each experiment was kept 0.02 g. The dishes containing catalysts were dried in an oven at 80 °C for about 4 h to evaporate the water and then cooled to room temperature before used. 20 mL RhB

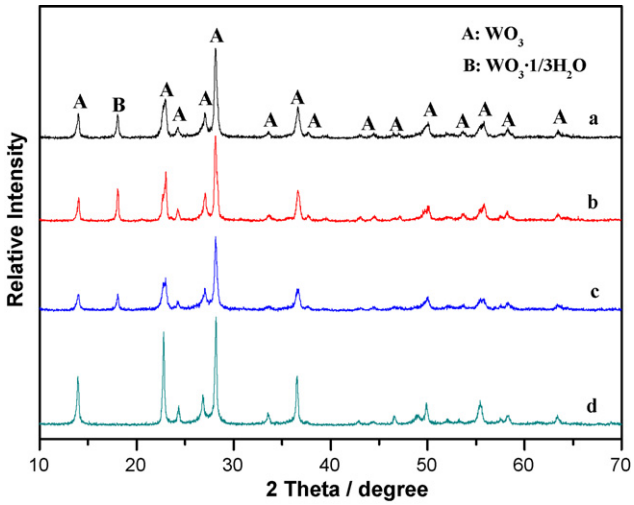

Fig. 1. XRD patterns of the samples: (a) W2, (b) W3, (c) W6 and (d) W7.

aqueous solution with a concentration of 1×10^{-5} M was added into the dishes coated with catalysts in each experiment. An 18 W daylight lamp (3 cm above the dish) was used as the light source, and the dish was covered with UV cutoff filter to completely remove any radiation below 400 nm and to ensure illumination by visible-light only. The concentration of RhB was determined by an UV-visible spectrophotometer (UV-2550, Shimadzu, Japan). Prior to irradiation, the dishes containing catalysts and RhB aqueous solution were kept in the dark for 40 min to ensure the establishment of an adsorption/desorption equilibrium between catalysts and RhB molecules. After daylight irradiation for 30 min, the reaction solution was separated to measure the concentration change of the RhB. As for the RhB aqueous solution with low concentration, its photocatalytic decolorization is a pseudo-first-order reaction and its kinetics may be expressed as [31,32]:

$$\ln\left(\frac{C_0}{C_t}\right) = kt \quad (1)$$

where k is the apparent rate constant, and C_0 and C_t are the RhB concentrations at $t = 0$ and $t = t$, respectively.

3. Results and discussions

3.1. Hierarchical assemblies of tungsten trioxide

Hierarchically flower-like tungsten trioxide assemblies were prepared through a simple one-step template-free hydrothermal method (see Section 2). The XRD pattern (Fig. 1a) of the sample W2 indicates that the sample contains two phases. All the peaks can be indexed as the hexagonal WO_3 (space group: $P6/mmm$; $a = 7.298$ Å, $b = 7.298$ Å, $c = 3.899$ Å, JCPDS no. 33-1387) and orthorhombic $WO_3{\cdot}(1/3)H_2O$ (space group: $Fmm2$; $a = 7.357$ Å, $b = 12.510$ Å, $c = 7.705$ Å, JCPDS no. 35-027) [33,34].

The morphology of the samples was investigated by SEM. Fig. 2 shows typical SEM images of the sample W2 at different magnification. The low magnification SEM image (Fig. 2a) clearly reveals that the product is composed of a lot of spherical flower-like particles with the size from 2 to 4 μm. Fig. 2b shows the morphology of an individual flower-like particle at a higher magnification SEM, indicating that such three-dimensional flowers are constructed from two-dimensional layers, which are further composed of lathy nanoflakes with irregular edges (Fig. 2c).

The hierarchically porous structures of the flower-like assemblies observed by SEM (Fig. 2) were further confirmed by BET analysis. Fig. 3 shows the nitrogen adsorption/desorption isotherms

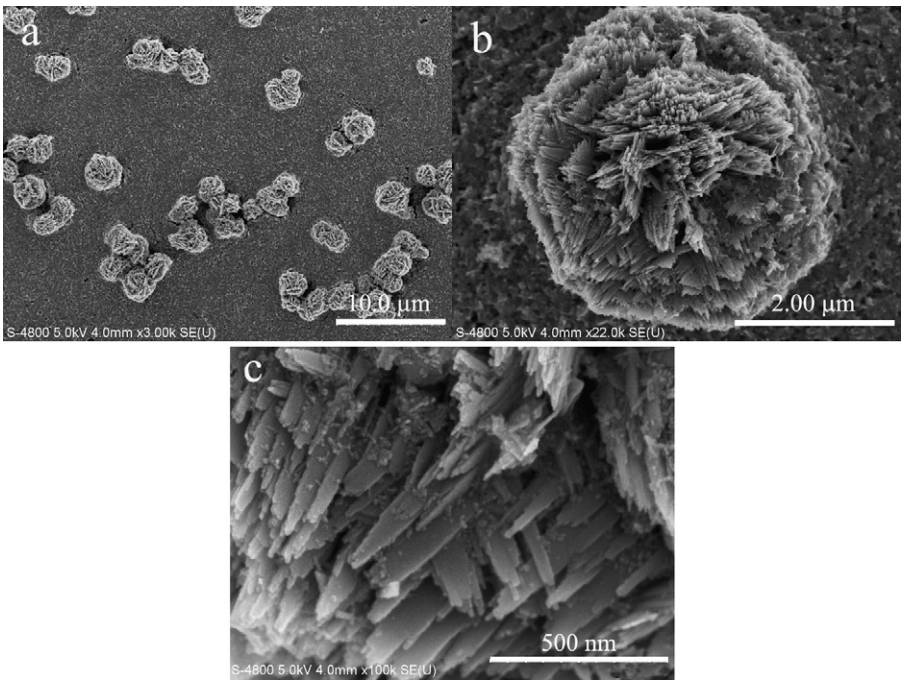

Fig. 2. SEM images of the sample W2 at different magnification.

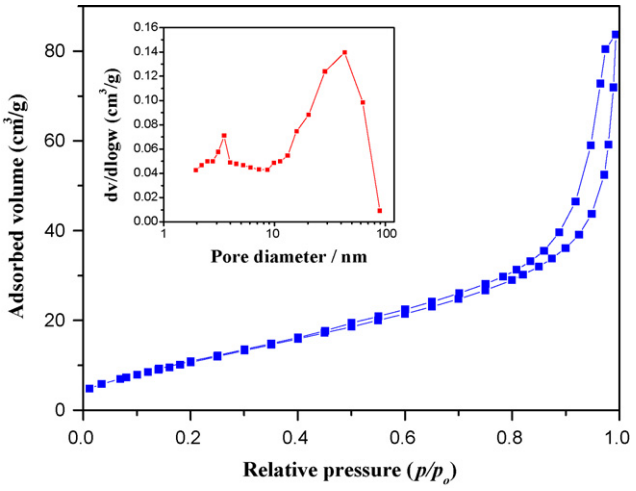

Fig. 3. Nitrogen adsorption–desorption isotherms and the corresponding pore size distributions curves (inset) of the sample W2.

and corresponding pore size distribution of flower-like tungsten trioxide assemblies. The nitrogen adsorption/desorption isotherm is of type IV and has two hysteresis loops, indicating bimodal pore size distribution in the mesoporous and macroporous regions. The shapes of the two hysteresis loops are different from each other. At low relative pressure between 0.4 and 0.7, the hysteresis loop is of type H2, suggesting the existence of ink-bottle pores with narrow necks and wider bodies (ink-bottle pores) [29]. However, at high relative pressure between 0.8 and 1.0, the shape of the hysteresis loop is of type H3 associated with aggregates of plate-like particles, giving rise to slitlike pores [29], which is consistent well with the SEM results. According to the previous reported results [35–37], a bimodal mesopore size distribution results from the different aggregates in the powders. The hysteresis loop in the low relative pressure range ($0.4 < P/P_0 < 0.7$) is related to finer intraaggregated pore formed between intraagglomerated primary crystallites, and that in higher relative pressure range ($0.8 < P/P_0 < 1$) is associated with larger interaggregated pore produced by inter-aggregated secondary particles. This bimodal pore size distribution is further confirmed by its pore size distribution (inset in Fig. 3). The flower-like tungsten trioxide assemblies contain small mesopores (peak pore, ca. 3.7 nm) and larger mesopores and macropores with a peak pore diameter of ca. 43 nm, corresponding to the voids between primary crystallites within the two-dimensional layers and the interspaces between these stacked layers, respectively. The pore structure parameters of the samples, such as specific surface area, pore volume, average pore size and porosity, are listed in Table 2.

3.2. Formation process

The time-dependent evolution experiments were carefully conducted to reveal the formation process of the hierarchically flower-like tungsten trioxide assemblies. The products collected at different reaction time from the reaction mixture were observed by SEM (as shown in Fig. 4). Fig. 4a shows that numerous nanoparticles first appeared at the initial stage (hydrothermal reaction 10 min). When the reaction reaches 30 min, a great number of nanoflakes and larger nanoparticles are produced (Fig. 4b). After

Table 2
Physical properties of the as-prepared samples.

Sample no.	Phase structures	S_{BET} (m^2/g)	Pore volume (cm^3/g)	Average pore size (nm)	Porosity %
W2	WO_3, $WO_3 \cdot (1/3)H_2O$	42.7	0.081	7.60	48.2
W3	WO_3, $WO_3 \cdot (1/3)H_2O$	43.6	0.089	8.17	48.9
W6	WO_3, $WO_3 \cdot (1/3)H_2O$	36.3	0.11	12.0	47.4
W7	WO_3	43.9	0.10	9.40	46.3

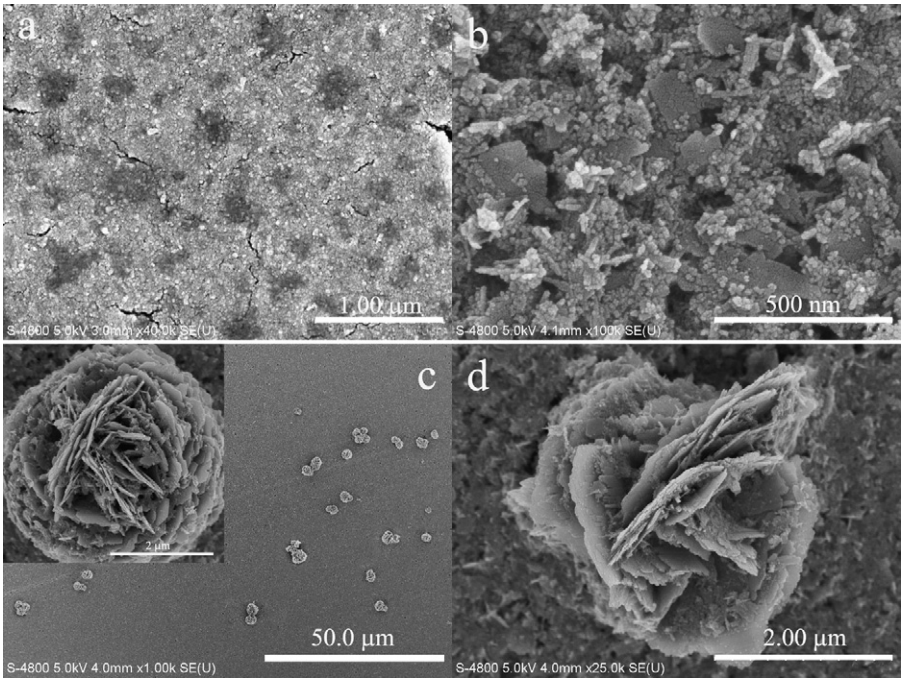

Fig. 4. SEM images of the sample W2 obtained at different reaction time: (a) 10 min, (b) 30 min, (c) and (d) 2 h.

2 h, many spherical flower-like assemblies 2–4 μm in size are obtained (Fig. 4c). These flower-like assemblies are formed via self-organization of two-dimensional nanoflakes with a mean thickness of ca. 10 and 60 nm in width. With further prolonging the reaction time to 24 h, these nanoflakes are changed into long and narrow ones with irregular edges (Fig. 2c).

On the base of the above results, we infer that the formation mechanism of hierarchically flower-like tungsten trioxide assemblies probably involves three steps (Fig. 5). After 10 min of hydrothermal reaction, a large number of nanoparticles are produced because high concentration at the initial stage is suitable for the rapid formation of small crystallites due to the domination of kinetic factor. When the hydrothermal time increases to 30 min, numerous nanoflakes and nanoparticles with different size appear (see Fig. 4b and step 1 of Fig. 5). It is well-known that although the formation of smaller crystallites is kinetically favored during the initial reaction stage, larger crystallites are thermodynamically favored [38]. Therefore, the primary small crystallites will self-aggregate and grow into large nanoparticles and nanoflakes through dissolution and recrystallization (Ostwald ripening). The formation of nanoflakes could be explained from the following factors as well. With increasing reaction time, the concentration of reactants decreases; an oriented dissolving step of inorganic nanoparticles occurs subsequently to form the plate-like building blocks for eliminating the higher surface energy faces. In addition, the gel formed after 10 min of reaction would facilitate the formation of nanoflakes, because it could provide the relatively stable environment for crystal growth. After 2 h of reaction, self-assembled flower-like superstructures with a diameter range from 2 to 4 μm are formed. Higher magnification SEM images of the flower-like assemblies show that these assemblies are constructed by many layers, which are further derived from wide flakes with rough surfaces and ragged edges (inset in Fig. 4c). Fig. 4d shows the higher magnification SEM image of an underdeveloped multilayer flower-like superstructure. It is interesting to note that some new layers are developing between the two preformed layers, and many branches grow on the surface and at edges of these layers. Liu proposed that the newborn layer could be the reason for the detachment and the curvature of initial closely stacked flat layers [39]. So, we suppose that the stacking and organizing of nanoflakes by dipole–dipole interactions and oriented attachment coupled simultaneously with their further growth and the development of new layers results in the formation of primary flower-like assemblies (step 2 in Fig. 5). According to the rule for crystal growth, secondary nucleation occurs preferentially at sites with more defects. Therefore, it is not surprising that some separated nanoflakes will grow from the preformed layers firstly, and subsequently give rise to the development of additional layers. Such process could make the assembled flowers more and more "flourishing" (see inset in Fig. 4c). When reaction time reaches to 24 h, the flower-like assemblies have no obvious change in size, but their building units change from wide nanoflakes into narrow and long nanoplates (Fig. 2c). As the concentrations of the reactants decrease gradually, the difference of growth rates at different sites becomes much greater. In detail, ragged edges of the layers and their rough surfaces are both energetically favorable integration sites for the ions of H^+ and WO_4^{2-}, which partly come from the dissolution of smaller crystalline. The preferential re-nucleation and continuous crystal growth at these energetically favorable sites will lead to the development of new plates, making the wide nanoflakes turn into "arrays of plates" (step 3 in Fig. 5). Finally, the progressive self-modification

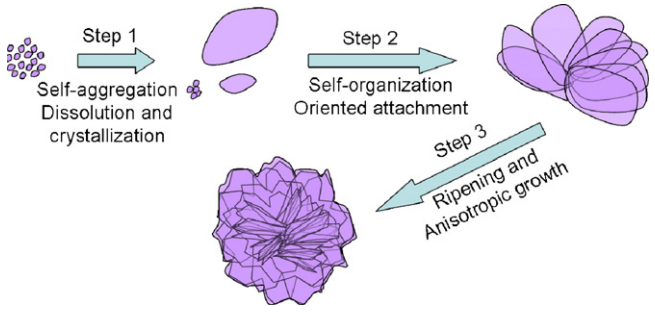

Fig. 5. Schematic illustration of the formation process of hierarchically tungsten trioxide flower-like assemblies.

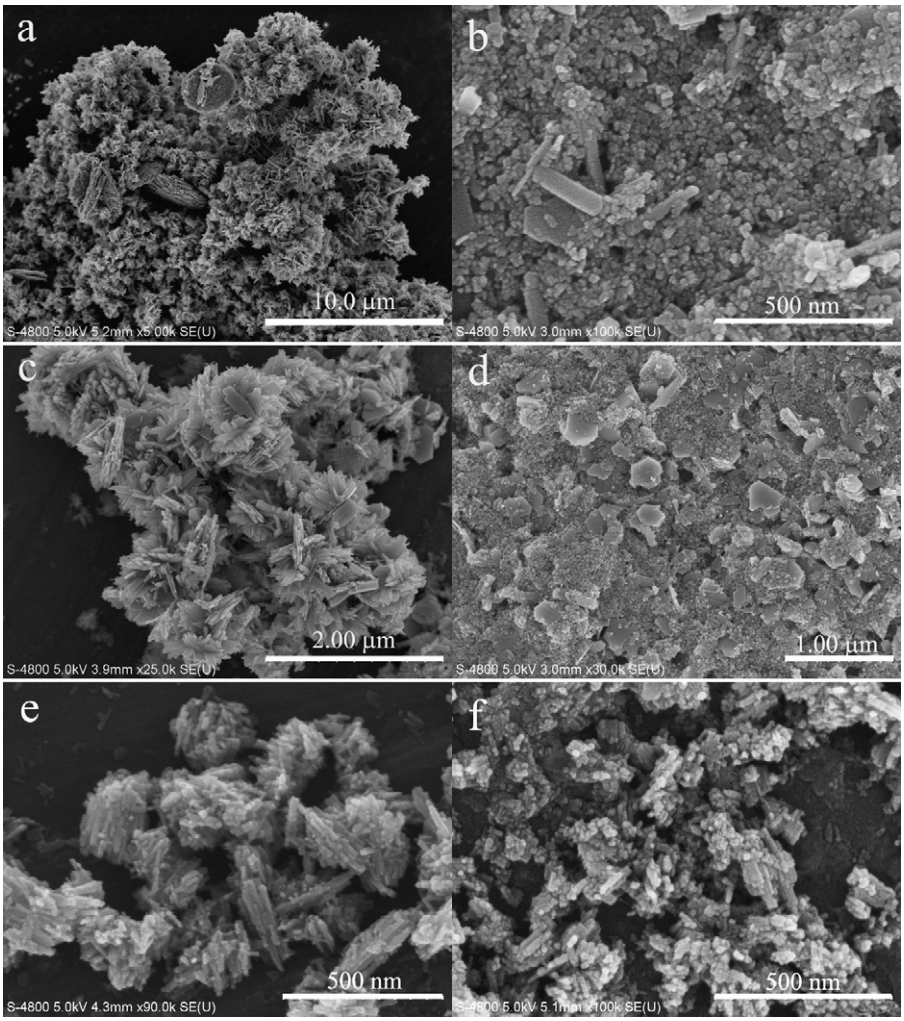

Fig. 6. SEM images of the samples prepared under different conditions: (a) W1, (b) W3, (c) W4, (d) W5, (e) W6 and (f) W7.

process occurs in the synthetic solution resulting in the ultimate flower-like configuration (Fig. 2c).

In order to systematically study the morphology evolution of tungsten trioxide, a series of control experiments was carried out (Table 1). Experimental results reveal that the concentrations of reactants and ***R*** have great influence on the morphology of the products. When ***R*** decreases to 0 or 1 (W8 and W9), no precipitate is obtained. Fig. 6(a) and (b) shows the SEM images of the samples W1 and W3 prepared at ***R*** = 1.5 and 3, respectively. At ***R*** = 1.5, some ill-defined morphology is observed (Fig. 6a). At ***R*** = 3, no hierarchically flower-like superstructures are obtained except some small particles and fragments (Fig. 6b). Therefore, an optimal ***R*** for the production of flower-like tungsten trioxide assemblies is 2. We also investigate the influence of reactant concentration on the morphology of tungsten trioxide. As the concentration of sodium tungstate varies from 0.003, 0.006 to 0.009 mol/L (at ***R*** = 2), the morphologies of tungsten trioxide evolve from nanoflakes aggregate (Fig. 6c) to flower-like assemblies (Fig. 2b) and then to separated nanoflakes (Fig. 6d). The results reveal that suitable initial concentration of reactants is crucial for the fabrication of hierarchically flower-like assemblies. In order to investigate the influence of different acid on the morphology of tungsten trioxide, other inorganic acids such as H_2SO_4 and HCl are also tested. Fig. 6(e) and (f) show the SEM images of the samples prepared in the presence of HCl and H_2SO_4, respectively. No hierarchically flower-like superstructures are obtained in these experiments. Therefore, this implies that the chemical natures of ionic species existed in the solution also have a great influence on the morphology of the final products, and the exact mechanism about these influence factors will be further investigated in our future works.

3.3. Photocatalytic activity

The visible-light photocatalytic activity of the hierarchically flower-like tungsten trioxide assemblies and the samples without such superstructures were evaluated and compared by photocatalytic decolorization of RhB aqueous solution. Illumination in the absence of tungsten trioxide samples did not result in the photocatalytic decolorization of RhB aqueous solution. After adsorption/desorption equilibrium between RhB molecules and the samples (40 min), the concentration of RhB did not change with increasing reaction time for every measurement using various tungsten trioxide samples under dark conditions without light illumination. Therefore, the presence of both light illumination and tungsten trioxide samples was necessary for the efficient photocatalytic degradation of RhB aqueous solution. These results also suggested that the degradation and decolorization of RhB aqueous solution was caused by photocatalytic reactions on tungsten trioxide samples under the visible-light illumination [31].

Fig. 7 displays the comparison of photocatalytic activity (apparent reaction rate constant or degradation percentage ratio) of the

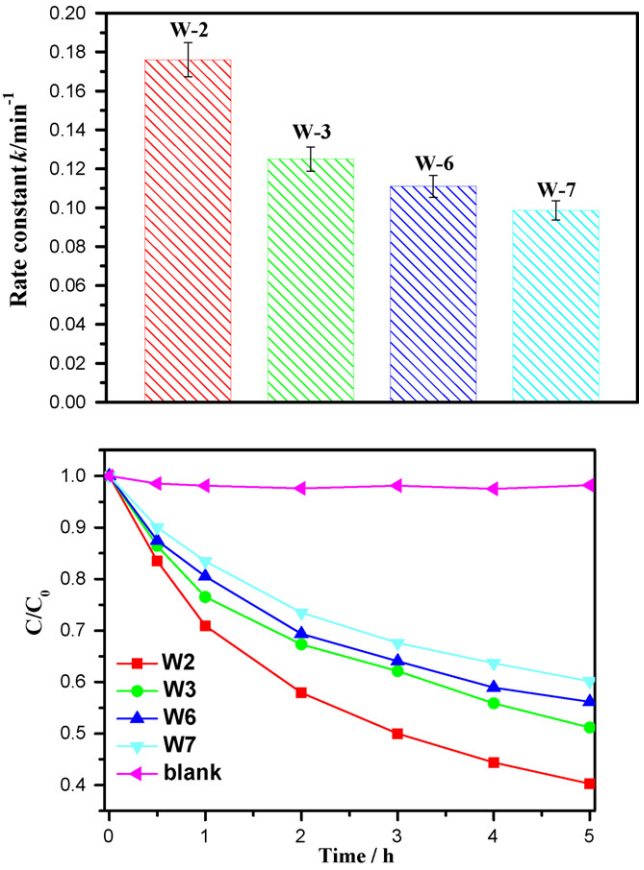

Fig. 7. Comparison of the photocatalytic activity of the samples: W2, W3, W6, W7 and blank tests, (a) apparent reaction rate constant and (b) degradation percentage ratio.

samples W2, W3, W6 and W7. It can be seen that the morphology of the samples has a great influence on the photocatalytic activity of tungsten trioxide samples. Although the sample W7 has the largest specific surface areas (see Table 2), there is a lowest photocatalytic activity observed due to the as-prepared tungsten trioxide powders consisting of single phase. For the sample W6, it has lowest specific surface areas, but it shows higher photocatalytic activity than the sample W7. This is due to its biphase structure (WO_3 and $WO_3{\cdot}(1/3)H_2O$). This also further confirms that the composite of two kinds of semiconductors or two phases of the same semiconductor is beneficial in enhancing photocatalytic activity due to reducing the combination rate of photogenerated electrons and holes [40–45]. For the sample W2, the highest photocatalytic activity is observed. The highest photocataytic activities of W2 might be explained by the composite structures of WO_3 and $WO_3{\cdot}(1/3)H_2O$, high specific surface areas and hierarchically bimodal macro-/mesoporous structures. Usually, for a photocatalyst, a large surface area could offer more active adsorption sites and photocatalytic reaction centers. The hierarchically macro-/mesoporous structures are beneficial to enhance the adsorption efficiency of light and the exchange rate of the reactant and product molecules. Therefore, it is not surprising that the sample W2 showed the highest photocatalytic activity among the prepared samples. Another possible explanation is that the sample W2 has an optimal ratio between the two phases of WO_3 and $WO_3{\cdot}(1/3)H_2O$ because the ratios of phases also obviously influence the photocatalytic activity of catalysts [6]. However, up to now, we have not a good method to determine the exact phase percentage in the samples. The sample W3 possesses a larger specific surface area than the sample W2. The increase in specific surface area should lead to an increase in the photocatalytic activity. However, the sample W3 exhibits relative lower photocatalytic activity than the sample W2. The decrease of photocatalytic activity of the sample W3 is due to the lack of hierarchically porous structures. The above results suggest that the morphology and phase structures of photocatalysts obviously influence their photocatalytic activity and the hierarchically porous superstructures could enhance the photoactivity of photocatalyst [6,8]. Therefore, to prepare highly active photocatalytic materials and to enhance the performance of photocatalyst, an efficient way would be to create the hierarchically porous structures in photocatalytic materials. The stability and recycling performance of photocatalysts are important factors for practical applications. To investigate the stability of the sample W2, several circulating runs in the photocatalytic degradation of RhB in the presence of W2 under visible-light irradiation were checked (Fig. 8). The photocatalytic activity does not exhibit any significant loss after five recycles for the photocatalytic degradation of RhB. It indicates that the hierarchically flower-like tungsten trioxide assemblies have high stability during the photocatalytic oxidation of RhB [42].

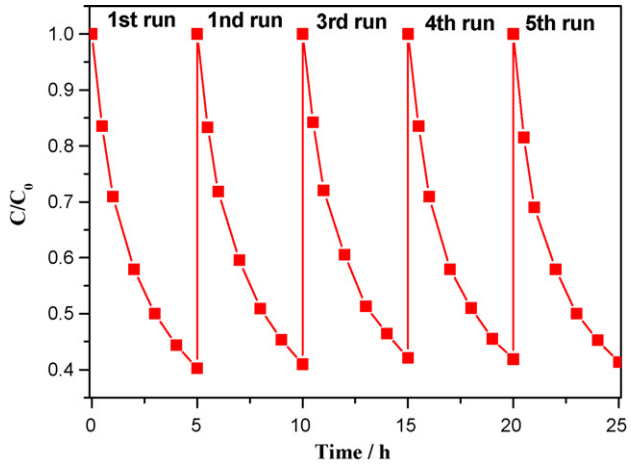

Fig. 8. Cycling runs in the photocatalytic degradation of RhB in the presence of W2 under visible-light irradiation.

4. Conclusion

Hierarchically flower-like tungsten trioxide superstructures are fabricated on a large scale by a simple hydrothermal method. The hierarchical structures endow the sample with hierarchical pores (bimodal mesopores). The peak pore at ca. 3.7 nm is associated with the voids between nanocrystallites within layers, while the peak pore at ca. 43 nm corresponds to the interspaces between stacked layers. The formation mechanism is a complex cooperation of self-organization, anisotropic growth, oriented attachment and Ostwald ripening. These hierarchically flower-like tungsten trioxide assemblies show higher visible-light photocatalytic activity than the sample without such hierarchical structures for the photocatalytic decolorization of Rhodamine B aqueous solution at ambient temperature, partly due to their specific hierarchical pores that serve as the transport paths for light and reactants. After five recycles for the photodegradation of RhB, the catalyst does not exhibit any great loss in activity, confirming hierarchically flower-like tungsten trioxide with high stability. This work might provide some new insights into the design of advanced photocatalytic materials with complex hierarchical architectures for enhancing visible-light-driven photocatalytic activity.

Acknowledgements

This work was partially supported by the National Natural Science Foundation of China (50625208, 20773097 and 20877061). This work was also financially supported by the National Basic Research Program of China (2007CB613302 and 2009CB939704).

References

[1] D. Simonsson, Electrochemistry for a cleaner environment, Chem. Soc. Rev. 26 (1997) 181.
[2] J.G. Yu, S.W. Liu, M.H. Zhou, Enhanced photocatalytic activity of hollow anatase microspheres by Sn^{4+} incorporation, J. Phys. Chem. C 112 (2008) 2050.
[3] M.R. Hoffmann, S.T. Martin, W. Choi, D.W. Bahnemann, Environmental applications of semiconductor photocatalysis, Chem. Rev. 95 (1995) 69.
[4] A.L. Linsebigler, G. Lu, J.T. Yates Jr., Photocatalysis on TiO_2 surfaces: principles, mechanisms, and selected results, Chem. Rev. 95 (1995) 735.
[5] P.V. Kamat, R. Huehn, R. Nicolaescu, "A Sense and Shoot" approach for photocatalytic degradation of organic contaminants in water, J. Phys. Chem. B 106 (2002) 788.
[6] J.G. Yu, L.J. Zhang, B. Cheng, Y.R. Su, Hydrothermal preparation and photocatalytic activity of hierarchically sponge-like macro-/mesoporous titania, J. Phys. Chem. C 111 (2007) 10582.
[7] F.B. Li, X.Z. Li, M.F. Hou, Photocatalytic degradation of 2-mercaptobenzothiazole in aqueous La^{3+}–TiO_2 suspension for odor control, Appl. Catal. B 48 (2004) 185.
[8] J.G. Yu, Y.R. Su, B. Cheng, Template-free fabrication and enhanced photocatalytic activity of hierarchical macro-/mesoporous titania, Adv. Funct. Mater. 17 (2007) 1984.
[9] J.G. Yu, X.J. Zhao, Q.N. Zhao, Effect of surface structure on photocatalytic activity of TiO_2 thin films prepared by sol–gel method, Thin Solid Films 379 (2000) 7.
[10] M.A. Fox, M.T. Dulay, Heterogeneous photocatalysis, Chem. Rev. 93 (1993) 341.
[11] H. Tada, M. Yamamoto, S. Ito, Promoting effect of MgO_x submonolayer coverage of TiO_2 on the photoinduced oxidation of anionic surfactants, Langmuir 15 (1999) 3699.
[12] A. Fujishima, T.N. Rao, D.A. Tryk, Titanium dioxide photocatalysis, J. Photochem. Photobiol. C 1 (2000) 1.
[13] K. Nagaveni, G. Sivalingam, M.S. Hegde, G. Madras, Photocatalytic degradation of organic compounds over combustion-synthesized nano-TiO_2, Environ. Sci. Technol. 38 (2004) 1600.
[14] H. Einaga, T. Ibusuki, S. Futamura, Improvement of catalyst durability by deposition of Rh on TiO_2 in photooxidation of aromatic compounds, Environ. Sci. Technol. 38 (2004) 285.
[15] X.T. Hong, Z.P. Wang, W.M. Cai, F. Lu, J. Zhang, Y.Z. Yang, N. Ma, Y.J. Liu, Visible-light-activated nanoparticle photocatalyst of iodine-doped titanium dioxide, Chem. Mater. 17 (2005) 1548.
[16] J.C. Yu, J.G. Yu, W.K. Ho, Z.T. Jiang, L.Z. Zhang, Effects of F^- doping on the photocatalytic activity and microstructures of nanocrystalline TiO_2 powders, Chem. Mater. 14 (2002) 3808.
[17] D. Le, A. Bellac, C.G. AZens, Granqvist, Angular selective transmittance through electrochromic tungsten oxide films made by oblique angle sputtering, Appl. Phys. Lett. 66 (1995) 1715.
[18] C.G. Granqvist, Electrochromic tungsten oxide films: review of progress 1993–1998, Sol. Energy Mater. Sol. Cells 60 (2000) 201.
[19] K. Bange, T. Gambke, Electrochromic materials for optical switching devices, Adv. Mater. 2 (1990) 10.
[20] M.D. Antonik, J.E. Schneider, E.L. Wittman, K. Snow, J.F. Vetelino, Microstructural effects in WO_3 gas-sensing films, Thin Solid Films 256 (1995) 247.
[21] X.L. Li, T.J. Lou, X.M. Sun, Y.D. Li, Highly sensitive WO_3 hollow-sphere gas sensors, Inorg. Chem. 43 (2004) 5442.
[22] J.G. Yu, H.G. Yu, H.T. Guo, M. Li, S. Mann, Spontaneous formation of a tungsten trioxide sphere-in-shell superstructure by chemically induced self-transformation, Small 4 (2008) 87.
[23] H. Hattori, N. Asada, K. Tanabe, Acidic property and catalytic activity of tungsten oxide, Bull. Chem. Soc. Jpn. 51 (1978) 1704.
[24] W. Morates, M. Cason, O. Aina, N.R. Tacconi, K. Rajeshwar, Combustion synthesis and characterization of nanocrystalline WO_3, J. Am. Chem. Soc. 130 (2003) 6318.
[25] M.A. Butler, R.D. Nasby, R.K. Quinn, Tungsten trioxide as an electrode for photoelectrolysis of water, Solid State Commun. 19 (1976) 1011.
[26] G. Hodes, D. Cahen, J. Manassen, Tungsten trioxide as a photoanode for a photoelectrochemical cell (PEC), Nature 260 (1976) 312.
[27] V. Luca, M.G. Blackford, K.S. Finnie, P.J. Evans, M.J. Lindsay, M. Skylas-kazacos, P.R.F. Barnes, Sol–gel tungsten oxide-titanium oxide multilayer nanoheterostructured thin films: structural and photoelectrochemical properties, J. Phys. Chem. C 111 (2007) 18479.
[28] Y. Guo, X. Quan, N. Lu, H. Zhao, S. Chen, High photocatalytic capability of self-assembled nanoporous WO_3 with preferential orientation of (002) planes, Environ. Sci. Technol. 41 (2007) 4422.
[29] K.S.W. Sing, D.H. Everett, R.A.W. Haul, L. Mosccou, R.A. Pierotti, J. Rouquerol, T. Siemieniewska, Reporting physisorption data for gas/solid systems with special reference to the determination of surface area and porosity, Pure Appl. Chem. 57 (1985) 603.
[30] E.P. Barrett, L.G. Joyner, P.H. Halenda, The determination of pore volume and area distributions in porous substances. I. Computations from nitrogen isotherms, J. Am. Chem. Soc. 73 (1951) 373.
[31] J.G. Yu, H.G. Yu, B. Cheng, X.J. Zhao, J.C. Yu, W.K. Ho, The effect of calcination temperature on the surface microstructure and photocatalytic activity of TiO_2 thin films prepared by liquid phase deposition, J. Phys. Chem. B 107 (2003) 13871.
[32] H. Kumazawa, M. Inoue, T. Kasuya, Photocatalytic degradation of volatile and nonvolatile organic compounds on titanium dioxide particles using fluidized beds, Ind. End. Chem. Res. 42 (2003) 3237.
[33] B. Gerand, G. Nowogrockl, M. Figlarz, A new tungsten trioxide hydrate, $WO_3 \cdot \frac{1}{3}H_2O$: preparation, characterization, and crystallographic study, J. Solid State Chem. 38 (1981) 312.
[34] M. Gotic, M. Ivanda, S. Popovic, S. Music, Synthesis of tungsten trioxide hydrates and their structural properties, Mater. Sci. Eng. B 77 (2000) 193.
[35] J.G. Yu, J.C. Yu, M.K.P. Leung, W.K. Ho, B. Cheng, X.J. Zhao, J.C. Zhao, Effects of acidic and basic hydrolysis catalysts on the photocatalytic activity and microstructures of bimodal mesoporous titania, J. Catal. 217 (2003) 69.
[36] J.G. Yu, G.H. Wang, B. Cheng, M.H. Zhou, Effects of hydrothermal temperature and time on the photocatalytic activity and microstructures of bimodal mesoporous TiO_2 powders, Appl. Catal. B 69 (2007) 171.
[37] K.N.P. Kumar, J. Kumar, K. Keizer, Effect of peptization on densification and phase-transformation behavior of sol–gel-derived nanostructured titania, J. Am. Ceram. Soc. 77 (1994) 1396.
[38] Y. Chang, J.J. Teo, H.C. Zeng, Formation of colloidal CuO nanocrystallites and their spherical aggregation and reductive transformation to hollow Cu_2O nanospheres, Langmuir 201 (2005) 1074.
[39] S.W. Liu, J.G. Yu, Cooperative self-construction and enhanced optical absorption of nanoplates-assembled hierarchical Bi_2WO_6 flowers, J. Solid State Chem. 181 (2008) 1048.
[40] J.G. Yu, Y.R. Su, B. Cheng, M.H. Zhou, Effects of pH on the microstructures and photocatalytic activity of mesoporous nanocrystalline titania powders, J. Mol. Catal. A 258 (2006) 104.
[41] J.G. Yu, S.W. Liu, H.G. Yu, Microstructures and photoactivity of mesoporous anatase hollow microspheres fabricated by fluoride-mediated self-transformation, J. Catal. 249 (2007) 59.
[42] J.G. Yu, X.X. Yu, Hydrothermal synthesis and photocatalytic activity of zinc oxide hollow spheres, Environ. Sci. Technol. 42 (2008) 4902.
[43] J.G. Yu, L.F. Qi, B. Cheng, X.F. Zhao, Effect of calcination temperatures on microstructures and photocatalytic activity of tungsten trioxide hollow microspheres, J. Hazard. Mater. 160 (2008) 621.
[44] Y.Q. Wu, G.X. Lu, S.B. Li, Study of preparation and photocatalytic activity of nanosized WO_3 powder, Acta Chim. Sin. 62 (2004) 1134.
[45] Y.X. Li, G.X. Lu, S.B. Li, Photocatalytic transformation of rhodamine B and its effect on hydrogen evolution over Pt/TiO_2 in the presence of electron donors, J. Photochem. Photobiol. A 152 (2002) 219.